Quantifying tumour hypoxia with fluorine-18 fluoroerythronitroimidazole ([18F]FETNIM) and PET using the tumour to plasma ratio

Kaisa Lehtiö[1], Vesa Oikonen[2], Samuel Nyman[2], Tove Grönroos[3], Anne Roivainen[1], Olli Eskola[4], Heikki Minn[1]

[1] Turku PET Centre, Turku University Central Hospital, PO Box 52, 20521 Turku, Finland
[2] Turku PET Centre, University of Turku, Turku, Finland
[3] Turku PET Centre, Medicity Research Laboratory, Turku, Finland
[4] Turku PET Centre, Radiopharmaceutical Chemistry Laboratory, Turku, Finland

Received: 21 June 2002 / Accepted: 5 September 2002 / Published online: 30 October 2002

Abstract. Fluorine-18 fluoroerythronitroimidazole ([18F]-FETNIM) is a nitroimidazole compound that is potentially useful as a hypoxia marker in positron emission tomography (PET) studies of oncological patients. Our aim was to develop a simple protocol to quantitate uptake of [18F]FETNIM in hypoxic tumours. Dynamic imaging data from ten patients with head and neck cancer undergoing [18F]FETNIM PET was used in simulations and model fits to assess hypoxia marker uptake under different levels of blood flow. The distribution volume determined from dynamic PET study was compared with simple tumour to plasma and tumour to muscle ratios at 90–120 min. In skeletal muscle having a low but variable blood flow [2–6 ml/(100 g×min)], differences in hypoxia-specific uptake of [18F]FETNIM remain small and may be hard to detect with PET. At higher blood flow [>20 ml/(100 g×min)], the retention of [18F]FETNIM reflects the oxygenation status well and results in satisfactory contrast between hypoxic and well-oxygenated tissue. A good estimate of tissue hypoxia is accomplished by measuring the tissue to plasma [18F]FETNIM activity ratio using only a few late time points. The increased hypoxia-specific retention of [18F]FETNIM in tissues with high blood flow, such as malignant tumours, may facilitate application of [18F]FETNIM as a hypoxia marker in oncological patients. In the assessment of the tumour to non-target uptake ratio, plasma is the preferred reference tissue rather than muscle, which may show a more heterogeneous tracer uptake not easily controlled for.

Keywords: Hypoxia – Radiotherapy – Modelling – PET – [18F]fluoroerythronitroimidazole

Kaisa Lehtiö (✉)
Turku PET Centre, Turku University Central Hospital, PO Box 52, 20521 Turku, Finland
e-mail: kaisa.lehtio@utu.fi
Tel.: +358-2-3130000, Fax: +358-2-2318191

Eur J Nucl Med (2003) 30:101–108
DOI 10.1007/s00259-002-1016-x

Introduction

Almost all solid tumours have a varying amount of hypoxic cells, representing viable cells adapted to a low oxygen concentration. The cells in a hypoxic microenvironment are resistant to radiotherapy and less accessible to several chemotherapeutic drugs [1]. It has recently been demonstrated that the hypoxic environment selects for more malignant phenotypes. Measuring the hypoxic fraction in tumours could enhance the development of hypoxia-targeted therapy and add to our understanding of the mechanisms associated with malignant progression [2].

Direct invasive measurement of oxygen concentration with polarographic needle electrodes has proved technically difficult and is limited to superficial tumours [3, 4]. Furthermore, these invasive probes may not be able to distinguish necrotic tumour cells from those that are anoxic but still viable. Therefore, interest has recently shifted towards techniques suited to the non-invasive measurement of tissue hypoxia. With positron emission tomography (PET) or single-photon emission tomography (SPET), radiolabelled hypoxia-avid compounds can be applied for the evaluation of oxygenation status in experimental or human tumours [5].

Nitroimidazoles are the most widely studied compounds for imaging hypoxia. [6]. Nitroimidazoles are reduced intracellularly in all viable cells and have an established use in the treatment of anaerobic infections. In aerobic cells the reduced nitroimidazole is immediately re-oxidised and washed out rapidly. By contrast, in cells with a low oxygen concentration the re-oxidation is slowed, which allows further reductive reactions to take

place. This leads to the formation of reactive products that can covalently bind to cell components or are charged and thus diffuse more slowly out of the tissue [6]. Casciari et al. [7] have developed a kinetic compartmental model to quantify tumour oxygenation status from PET data using fluorine-18 labelled fluoromisonidazole ([^{18}F]FMISO, 1-(3-[^{18}F]fluoro-2-hydroxypropyl)-2-nitroimidazole), the nitroimidazole compound most widely used in clinical PET. The kinetic model of [^{18}F]FMISO cellular bioreduction relates cellular oxygen concentration to the cellular [^{18}F]FMISO reaction rate constant, κ_A.

We are currently studying the use of fluorine-18 labelled fluoroerythronitroimidazole ([^{18}F]FETNIM, 1-(2,3-dihydroxy-4-[^{18}F]fluorobutyl)-2-nitroimidazole), a nitroimidazole compound first synthesised by Yang et al. [8], in the imaging of hypoxia in human head and neck cancer [9, 10]. Since the irreversible, covalent binding of nitroimidazoles to cellular macromolecules has been considered the principal mechanism of accumulation in the hypoxic cells [11, 12], we first attempted to fit a model for irreversibly trapping tracers, developed by Patlak and Blasberg [13]. However, we constantly failed to produce a linear plot with a positive slope, as would have been expected for tracers with predominantly irreversible uptake. We then decided to adapt the model introduced by Logan et al. [14, 15] and originally used in receptor studies for reversible trapping of tracers. The fits using Logan's model showed linear plots and encouraged us to explore [^{18}F]FETNIM uptake characteristics in more detail.

In clinical studies it has been demonstrated that the macromolecular bound fraction of misonidazole shows dose dependency and is no more than 23% of a given dose [12, 16]. In these in vitro studies the nitroimidazole dose range of 1–25 μ*M* was an order of magnitude higher than the dose (~20 pmol/kg) given to a patient in our previous PET study [9]. Our calculation of a picomolar nitroimidazole concentration is based on a quotient of injected radioactive dose of approximately 370 MBq, and a specific radioactivity higher than 300 GBq/μmol for a 70-kg person.

Accurate validation showing that a given radionuclide method truly measures hypoxia in vivo is problematic [17]. Attempts have been made to correlate tracer uptake with the results of other methods which evaluate oxygen content in tissue, such as microelectrode measurements of the oxygen partial pressure (pO_2), pO_2 luminescence and phosphorus-31 nuclear magnetic resonance spectroscopy [18, 19]. These other assays measure the tissue oxygenation in small subvolumes of the tumour and are rather sensitive to the presence of necrosis. In general, no strong correlation exists between hypoxia marker uptake and the other assays measuring tissue oxygenation [20, 21]. Also, hypoxia marker uptake has been studied using modulations of the oxygenation status by vasoactive agents or different breathing gases. Significant correlations have been found [22, 23, 24] but these modulations alter both delivery of the hypoxic marker and delivery of oxygen to the tissue, and appropriate corrections are difficult to make. The preferred validation technique in animal tumours is the measurement of tissue radioresistance, but this assay is difficult to apply in human studies [5, 25].

At present, our group is performing preclinical studies to verify that [^{18}F]FETNIM uptake reflects the hypoxia in tissue, and preliminary results have been encouraging. However, to interpret the data more precisely, we have used simulations in the present study to assess the relative effects of blood flow and hypoxia on the tissue uptake of [^{18}F]FETNIM. These simulations are based on the actual PET data measured from patients with head and neck cancer. Furthermore, with the simulations we have aimed to simplify the PET study in the clinical setting to permit use of a short imaging protocol coupled with only a few blood samples. Our experience with dynamic [^{18}F]FETNIM PET imaging suggests that reversible trapping may play a more important role in the evaluation of nitroimidazole uptake than previously thought. With the simulations we show that even moderate irreversible binding, as assumed in the applied compartmental model [7], does not compromise the use of the simple quantification method presented in this study.

Materials and methods

The [^{18}F]FETNIM tumour tissue and arterial plasma time-activity data of ten patients collected for another protocol were analysed in this study. The radiochemical syntheses of [^{18}F]FETNIM and [^{15}O]H_2O and the PET acquisition protocol have been explained in detail in previous publications [9, 10]. In brief, all patients had a histologically verified squamous cell carcinoma in the head and neck region, and they were studied prior to the start of the cancer treatment. All patients gave written informed consent before entering the study, and the imaging protocol was reviewed and accepted by the joint ethical committee of Turku University and Turku University Central Hospital. First, all ten patients underwent a dynamic blood flow measurement using [^{15}O]H_2O with a median dose of 1,152 MBq (range 821–1,800 MBq). Secondly, a median dose of 365 MBq of [^{18}F]FETNIM (range 289–385 MBq) was injected as a 15-s bolus and two imaging protocols were employed. Six patients were studied for 120 min continuously from the time of injection. The other four patients were studied from 0 to 20 min post injection; after a 60-min rest period a second 40-min scan was performed to obtain the data 80–120 min post injection. Regions of interest (ROIs) were drawn on muscle and tumour tissue as previously described [9] to obtain the regional time-activity data. Because of the heterogeneity of tumour tissue, a maximum area of 3×3 pixels (7.04×7.04 mm) inside each tumour region was also determined, representing the highest area under the radioactivity concentration curve.

The tumour and plasma time-activity curves were used to determine the equilibrium distribution volume (DV) of [^{18}F]FETNIM, applying the graphical method developed by Logan et al. [14] as explained in our previous study [9]. In addition, the ratios of tissue and plasma radioactivity concentrations at the end of the

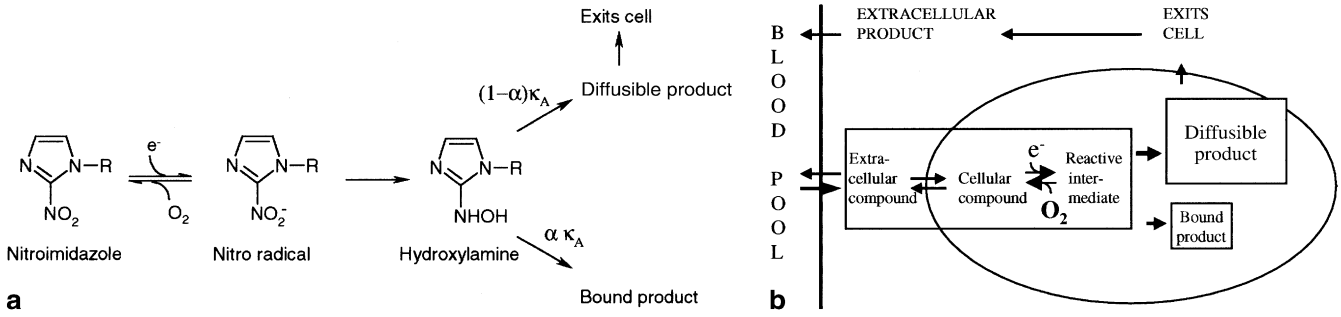

Fig. 1. a A simplified kinetic model of nitroimidazole bioreduction reactions. α is the fraction of the nitroimidazole that forms the bound product, and κ_A is the cellular reaction rate constant of the nitroimidazole compound. *R* denotes the variable carbon side chain of different nitroimidazole compounds. **b** The compartmental model of nitroimidazole transport and metabolism. Both figure parts are modified from Casciari et al. [7]

dynamic acquisition (90–120 min after injection) were calculated. We assumed this ratio to be related to the Logan DV even though we had given the tracer as a bolus instead of by means of a constant infusion, as is in theory required for a true equilibrium state between tissue and plasma. Calculation of the tissue to plasma ratio is an attractive method for wider clinical and diagnostic use, since it requires only a short imaging schedule at an appropriate time after injection and a few venous blood samples. Finally, a compartmental model for another nitroimidazole [^{18}F]FMISO, introduced by Casciari et al. [7], was applied to analyse the current [^{18}F]FETNIM PET data. The lower lipophilicity of [^{18}F]FETNIM can be expected to affect the rate constants of the model, but not to invalidate the model as such. The behaviour of nitroimidazoles and the compartmental model are described in Fig. 1 and the derived mathematical equations are shown in the Appendix. As suggested by Casciari et al. [7], the model parameters V_T, α, η and κ_B were constrained to values 1.0, 0.36, 0.50 and 0.013, respectively, and the parameters *F*, β_1, β_2 and κ_A were estimated by the non-linear least-squares optimisation procedure for each tumour region. For a full explanation of model parameters, see the Appendix.

The estimation of compartmental model parameters from the measured tumour and muscle PET data gave a range of values which were used to simulate the relative dependence of the tissue to plasma ratio on hypoxia and blood flow. A representative plasma curve was selected and used as an input in simulations. Tissue curves were simulated by applying the model equations given in the Appendix and the median values of estimated model parameters, changing the parameters representing hypoxia (κ_A) and blood flow (*F*) when necessary. These simulated tissue curves were then used to calculate the tissue to plasma ratio and to plot the ratio as a function of hypoxia or blood flow.

Pearson's correlation coefficients (*r*) and the corresponding *P* values were calculated using MicroCal Origin 6.0 software (Northampton, Mass.). Since parameters calculated from tumour data show considerable variation not representing Gaussian distribution, median values instead of means are shown.

Results

The blood flow, distribution volumes and tissue to plasma ratios calculated for total tumour regions and maximum areas within them, as well as for muscle regions used as reference regions, are shown in Table 1. The

Table 1. Patient data

Patient	Blood flow [ml/(100 ml×min)]		Tissue to plasma [^{18}F]FETNIM uptake ratio				[^{18}F]FETNIM DV[b]	
	Tumour	Muscle	Tumour (maximum)	Tumour (whole)	Muscle	Tumour[a]/ muscle	tumour (maximum)	muscle
1	35.3	6.2	0.91	0.74	0.57	1.29	0.85	0.54
2	44.4	2.2	1.41	1.00	0.50	2.00	1.20	0.44
3	48.4	4.1	0.94	0.79	0.53	1.49	0.91	0.49
4	63.1	2.2	1.98	1.10	0.83	1.32	1.64	0.72
5	44.9	4.4	1.49	1.06	0.67	1.58	1.22	0.56
6	23.7	3.5	1.24	0.95	0.81	1.18	1.08	0.76
7	29.6	2.9	1.34	0.96	0.59	1.64	1.21	0.52
8	ND	ND	1.07	0.92	0.54	1.69	0.99	0.50
9	37.0	2.7	1.22	0.99	1.15	0.86	1.15	0.99
10	14.1	2.4	1.50	0.87	0.71	1.23	1.20	0.56
Median	37.0	2.9	1.29	0.96	0.63	1.41	1.18	0.55

ND, Not determined
[a]Whole tumour
[b]According to the Logan method
** ND, Not determined

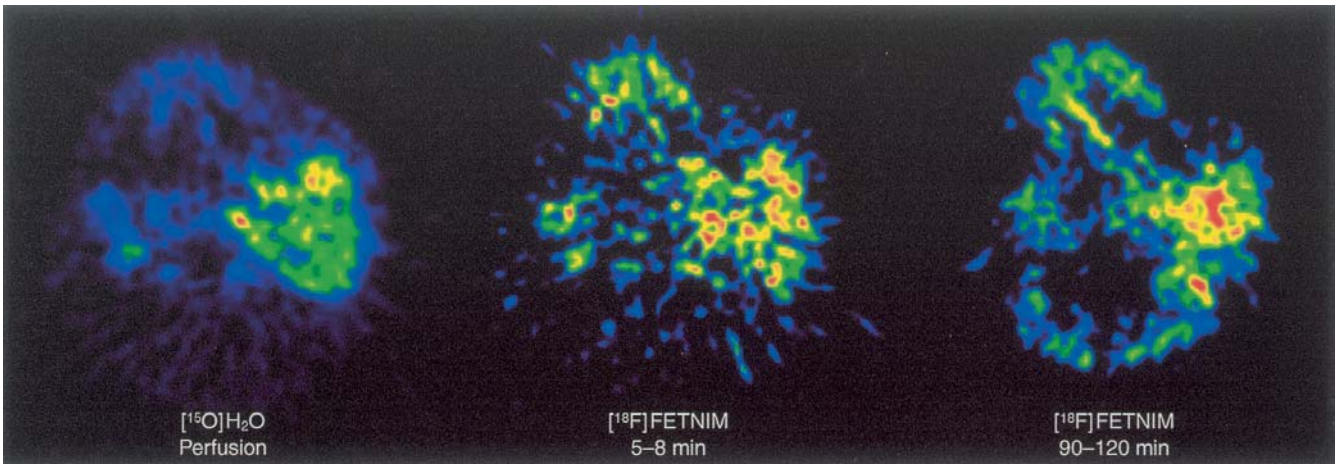

Fig. 2. Perfusion and [18F]FETNIM PET images of a patient with a left hypopharyngeal tumour. Note the different pattern of distribution of uptake of [18F]FETNIM in the early and late phases of the dynamic study

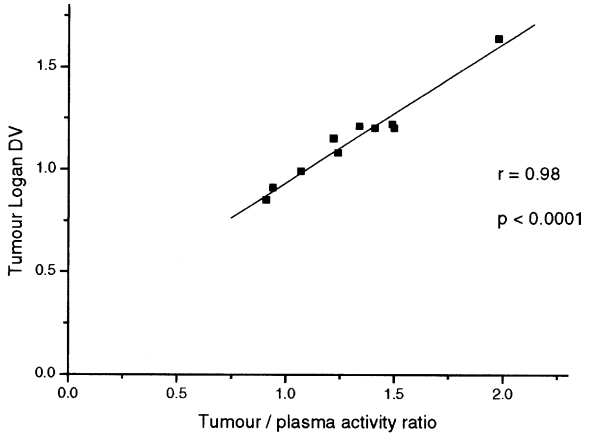

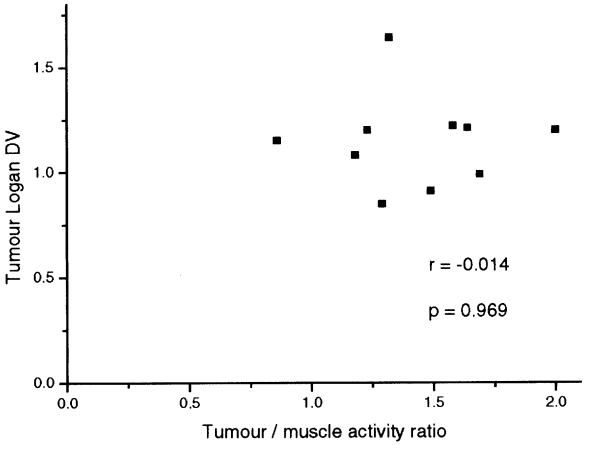

Fig. 3. a The correlation between the tumour [18F]FETNIM distribution volume (DV) using Logan analysis and the tumour to plasma [18F]FETNIM activity ratio. **b** The tumour [18F]FETNIM DV plotted against the tumour to muscle activity ratio shows no correlation between the two measures

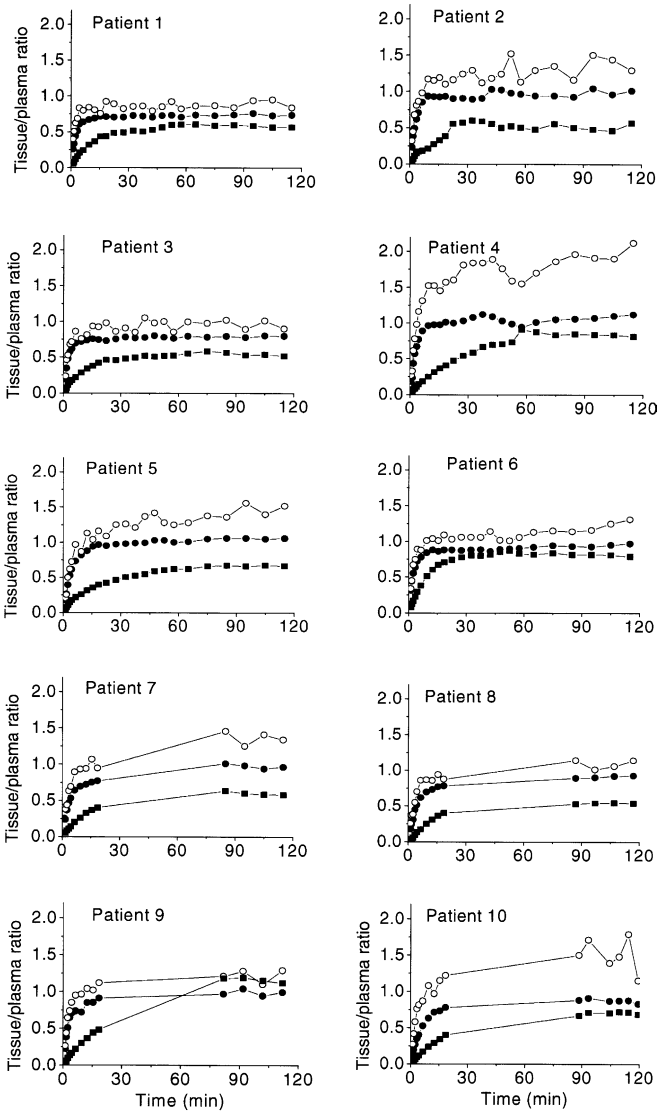

Fig. 4. The tissue to plasma activity concentration ratio as a function of time derived from all individual [18F]FETNIM PET studies. Measurements are shown for whole tumour (*closed circles*), in the maximal uptake area within tumour (*open circles*) and in muscle (*closed squares*)

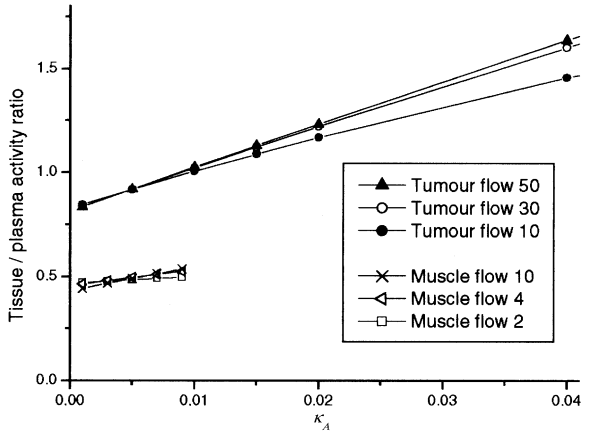

Fig. 5. Tissue to plasma activity ratio as a function of κ_A, the cellular reaction rate constant, for different flow values [ml/(100 ml×min)] simulated for both tumour and muscle. In tumour the change in the κ_A value (representing the hypoxia level) has a much larger effect on the tissue to plasma ratio than does a change in the blood flow level, whereas in muscle the change in the κ_A level has almost no effect on the tissue to plasma ratio at the flow levels assumed to be typical for resting skeletal muscle

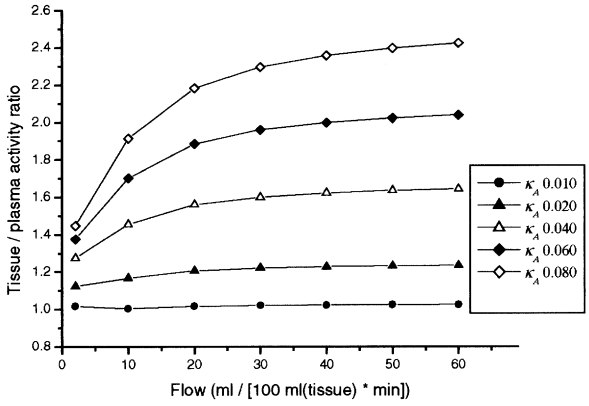

Fig. 6. Tissue to plasma [^{18}F]FETNIM ratio as a function of blood flow calculated from simulated tumour activity curves at 120 min after injection. The five κ_A values represent different levels of hypoxia expressed as percentage of [^{18}F]FETNIM bound to irreversible or reversible compartments. In the flow range likely to be typical for head and neck tumours [20–50 ml/(100 ml×min)], the change in flow has only a minor effect on the tissue to plasma ratio, whereas in the flow range of muscle tissue [2–10 ml/(100 ml×min)], the change in flow has a much larger effect on the tissue to plasma ratio than does that in κ_A

Table 2. Fitted parameter values

Patient	Flow	β_1	β_2	κ_A
1	0.17	0.26	0.50	0.003
2	0.20	0.16	0.78	0.013
3	0.23	0.19	0.55	0.009
4	0.60	0.18	0.96	0.004
5	0.14	0.16	0.77	0.014
6	0.23	0.16	0.66	0.015
7	0.27	0.19	0.62	0.008
8	0.21	0.27	0.60	0.015
9	0.21	0.23	0.61	0.010
10	0.23	0.07	0.70	0.016
Median	0.22	0.19	0.64	0.012

PET images of a patient with hypopharyngeal cancer are shown in Fig. 2. The blood flow as measured with the [^{15}O]H_2O bolus technique in tumour was always several times higher than that in muscle. The median tumour blood flow was 37.0 ml/(100 ml×min) and the median muscle blood flow was 2.9 ml/(100 ml×min). The tumour [^{18}F]FETNIM DV calculated using the Logan method correlated excellently with the tumour-to-plasma activity ratio (r=0.98, P<0.0001) (Fig. 3a). On the other hand the tumour-to-muscle activity ratio did not correlate at all with the Logan DV for [^{18}F]FETNIM (r=–0.014, P=0.969) (Fig. 3b). The tissue to plasma ratios reached a steady state level after about 60 min post injection in all studied patients, in both tumour tissue and in muscle (Fig. 4). The estimated compartmental model parameter values are shown in Table 2. Although the model fits were excellent, the high variability discourages use of the individual values.

The simulation of the dependence of the tissue to plasma ratio at 120 min on tissue hypoxia is shown in Fig. 5, and the effect of blood flow on this ratio is shown in Fig. 6. At the predicted range of blood flow values occurring in tumours, the tissue to plasma ratio is more dependent on hypoxia than on blood flow. By contrast, at the oxygenation levels expected to prevail in resting muscle, the tissue to plasma ratios seem to be rather insensitive to changes in hypoxia.

Discussion

The existence of viable tumour cells in a hypoxic microenvironment compromises the outcome of conventional cancer treatment. The quantitative measurement of tumour hypoxia in vivo assists in the development of treatments specifically targeting these seemingly resistant cells. Radionuclide imaging has been recognised as a promising tool to detect hypoxic cells which can then be exposed to strategies to modify radioresistance.

We are currently exploring the possibilities of imaging tumour hypoxia with PET using a hydrophilic nitroimidazole compound, [^{18}F]FETNIM. [^{18}F]FETNIM shows rapid washout of unmetabolised tracer from well-oxygenated non-target tissues via the urinary tract [10]. It is assumed that low oxygen concentration is a prerequisite for [^{18}F]FETNIM binding and that [^{18}F]FETNIM PET results in an inverse image of tissue oxygenation. The validation of any quantitative method to determine the hypoxic fraction in human tumours has turned out to

be arduous [17]. However, the events that cannot be measured non-invasively at the microscopic level can be predicted on the basis of simulations and prior knowledge of nitroimidazole metabolism.

In our simulations we decided to use real plasma curves and measurements of blood flow in both muscle and tumour, which were obtained using [^{15}O]H_2O PET and [^{18}F]FETNIM PET performed in sequential fashion. Since [^{18}F]FETNIM is metabolised only to a limited degree in patients [10], the arterial plasma curves were not corrected for metabolites. From the simulations we observed that the tissue blood flow level has a notable effect on the model's function. If the blood flow in tissue is low, tracer uptake is rather insensitive to changes in oxygen concentration, whereas in cases of high perfusion, the level of hypoxia becomes the major determinant of the tissue to plasma activity ratio (Fig. 6). In other words, it is much harder to detect hypoxia with [^{18}F]FETNIM PET in, for example, resting skeletal muscle, which usually has low perfusion, than in head and neck cancer, heart, and brain, in which blood flow is adequate for hypoxia-specific imaging. Furthermore, tracer is quickly washed out from normoxic tissues under high perfusion in comparison to similarly oxygenated areas where blood flow is, say, between 5 and 10 ml/(100 ml×min). The variability in blood flow of skeletal muscle may affect [^{18}F]FETNIM uptake although the latter may be difficult to assess reliably during the different phases of the PET acquisition (Table 1, Fig. 4). An unexpected increase in muscle blood flow can be caused by, for example, tension in neck muscles or stress during the long imaging session. The variability in muscle blood flow and the poor correlation between tumour distribution volume and tumour to muscle ratio (Fig. 3b) indicate that muscle is an unreliable reference tissue in imaging hypoxia, at least when using [^{18}F]FETNIM. Furthermore, the presence of hypoxia in muscle especially in the later phases of long imaging schedules cannot be ruled out (Fig. 4).

Our fitted κ_A values, which represent hypoxia, may seem to be rather small (range 0.003–0.016, see Table 2). It should be noted, however, that they are means of the whole tumour, and regionally the values may be much larger owing to the heterogeneous nature of tumour tissue. Therefore, we have also simulated much higher κ_A values which should represent the more hypoxic and radioresistant tumour cells. Our measured data which show approximately 1.2- to 2-fold differences in mean and maximum tumour to plasma ratios suggest that κ_A values higher than 0.06 can be expected to occur if the assumptions of the model are correct in general. As Fig. 6 indicates, simultaneous measurement of flow and late [^{18}F]FETNIM binding would improve assessment of κ_A. Clinically this might be accomplished by using the initial phase of [^{18}F]FETNIM uptake for the measurement of flow and later the steady-state phase for the measurement of hypoxia-specific uptake [9].

In the compartmental model for [^{18}F]FMISO, Casciari et al. [7] assumed that the fraction of irreversible [^{18}F]FMISO binding (α) is 36%. We have adopted the same value in our model fits and simulations for [^{18}F]FETNIM. However, we expect that in practice the fraction of radioactivity in the reversible compartment may contribute more significantly to the uptake of [^{18}F]FETNIM and [^{18}F]FMISO than is assumed in the simulations. This is supported by our findings [9] that graphical analysis for determining the distribution volume of reversible PET tracers [14, 15] can be applied to [^{18}F]FETNIM data, and that the tissue to plasma ratios tend to reach a plateau during the PET study (Fig. 4). The previous literature has also suggested that irreversible binding is not the major mode of accumulation of the nitroimidazoles. As Nunn et al. have pointed out [6], formation of the less permeable compounds is sufficient for transient trapping of an imaging agent. Since the relative importance of reversible versus irreversible binding of nitroimidazoles remains unclear, measures like the tissue to plasma ratio that depict the total tissue tracer uptake independent of the exact uptake mechanism seem to be the preferred means for the quantification of hypoxia.

At first it may seem confusing that under high blood flow in a tumour, a considerable fraction of hypoxic cells may still exist. Hypoxia is a strong stimulus for angiogenesis, and by itself increases the neovascularisation of the tissue. Tumour perfusion is highly heterogeneous, and tumour blood vessels are very irregular and tortuous, with many blind ends and arteriovenous shunts. Furthermore, these blood vessels have incomplete endothelial linings and basement membranes and they lack smooth muscle and innervation [26]. As a result, there can be a lot of non-nutritive blood flow in the tumour, equivalent to a well-known phenomenon called luxury perfusion. Our [^{15}O]H_2O autoradiographic method for the measurement of blood flow represents the sum of plasma flow and red blood cell flow in the tissue. Given the chaotic architecture of the blood vessels, in tumours there can be regions where the oxygenated red blood cells cannot pass although plasma enters easily. This will result in high apparent blood flow but low oxygen delivery.

Conclusion

We have studied a nitroimidazole compound, [^{18}F]FETNIM, to assess its applicability in imaging hypoxia quantitatively in human head and neck cancer. Our approach was to simulate different levels of hypoxia and blood flow based on previous studies and our own patient data. As a result a model of the nitroimidazole metabolism in tissue has been presented, where reversible binding of the tracer into the intracellular compartment represents the majority of the radioactivity in hypoxic cells. We recommend the use of plasma activity as a reference tissue instead of muscle since the latter is more

heterogeneous between patients, and may be sensitive to changes in blood flow and show temporal changes in oxygenation.

Acknowledgements. We thank the medical laboratory technologists and radiographers of the Turku PET Centre for their skilful assistance and co-operation. Financial support was provided in part by the Finnish Cancer Foundation, the Southwestern Finnish Cancer Foundation and the Turku University Foundation.

Appendix

Casciari et al. [7] developed a compartmental model for [^{18}F]fluoromisonidazole (FMISO), here applied for [^{18}F]FETNIM. The equations for describing the mass balance of FETNIM and its metabolites in the tissue using their nomenclature, after correction of two inconsistencies, are:

$$\frac{dC_c(t)}{dt} = \frac{F}{V_T}\left(C_p(t) - C_c(t)\right) - (1-\eta)\,\kappa_A C_c(t)$$

$$\frac{dC_{bp}(t)}{dt} = \alpha\kappa_A C_c(t)$$

$$\frac{dC_{dp}(t)}{dt} = (1-\alpha)\,\kappa_A C_c(t) - \kappa_B C_{dp}(t)$$

$$\frac{dC_{dpe}(t)}{dt} = \frac{1-\eta}{\eta}\kappa_B C_c(t) - \frac{F}{\eta V_T} C_{dpe}(t)$$

$$A(t) = \beta_1 C_p(t) + \beta_2 V_T\left(C(t) + (1-\eta)\,C_{bp}(t) + (1-\eta)\,C_{dp}(t) + \eta C_{dpe}(t)\right)$$

Abbreviations

C_c	[^{18}F]FETNIM concentration in the tissue
C_{bp}	Cellular bound product
C_{dp}	Cellular diffusible product
C_{dpe}	Extracellular diffusible product
$A(t)$	Total activity
C_p	[^{18}F]FETNIM concentration in the blood plasma
F	Blood flow rate
V_T	Tissue-specific volume
η	Fraction of tissue-specific volume occupied by extracellular space
α	Fraction of [^{18}F]FETNIM binding that forms bound product
β_1, β_2	Tissue activity correction factors (accounting for spillover and partial volume effects in PET measurements)
κ_A	Cellular [^{18}F]FETNIM reaction rate constant
κ_B	Rate constant for efflux of diffusible products out of the cell

References

1. Hall EJ. Radiosensitizers and bioreductive drugs. In: Hall EJ, ed. *Radiobiology for the radiologist.* Philadelphia: Lippincott; 1994:165–181.
2. Brown JM. Exploiting the hypoxic cancer cell: mechanisms and therapeutic strategies. *Mol Med Today* 2000; 6:157–162.
3. Nordsmark M, Bentzen SM, Overgaard J. Measurement of human tumour oxygenation status by a polarographic needle electrode. An analysis of inter- and intratumour heterogeneity. *Acta Oncol* 1994; 33:383–389.
4. Nordsmark M, Overgaard M, Overgaard J. Pretreatment oxygenation predicts radiation response in advanced squamous cell carcinoma of the head and neck. *Radiother Oncol* 1996; 41:31–39.
5. Chapman JD, Schneider RF, Urbain JL, Hanks GE. Single-photon emission computed tomography and positron-emission tomography assays for tissue oxygenation. *Semin Radiat Oncol* 2001; 11:47–57.
6. Nunn A, Linder K, Strauss HW. Nitroimidazoles and imaging hypoxia. *Eur J Nucl Med* 1995; 22:265–280.
7. Casciari JJ, Graham MM, Rasey JS. A modeling approach for quantifying tumor hypoxia with [F-18]fluoromisonidazole PET time-activity data. *Med Phys* 1995; 22:1127–1139.
8. Yang DJ, Wallace S, Cherif A, Li C, Gretzer MB, Kim EE, Podoloff DA. Development of F-18-labeled fluoroerythronitroimidazole as a PET agent for imaging tumor hypoxia. *Radiology* 1995; 194:795–800.
9. Lehtiö K, Oikonen V, Grönroos T, Eskola O, Kalliokoski K, Bergman J, Solin O, Grénman R, Nuutila P, Minn H. Imaging of blood flow and hypoxia in head and neck cancer: initial evaluation with [^{15}O]H_2O and [^{18}F]Fluoroerythronitroimidazole PET. *J Nucl Med* 2001; 42:1643–1652.
10. Grönroos T, Eskola O, Lehtiö K, Minn H, Marjamäki P, Bergman J, Haaparanta M, Forsback S, Solin O. Pharmacokinetics of [^{18}F]FETNIM: a potential marker for PET. *J Nucl Med* 2001; 42:1397–1404.
11. Varghese AJ, Whitmore GF. Binding to cellular macromolecules as a possible mechanism for the cytotoxicity of misonidazole. *Cancer Res* 1980; 40:2165–2169.
12. Chapman JD, Baer K, Lee J. Characteristics of the metabolism-induced binding of misonidazole to hypoxic mammalian cells. *Cancer Res* 1983; 43:1523–1528.
13. Patlak CS, Blasberg RG. Graphical evaluation of blood-to-brain transfer constants from multiple-time uptake data. Generalizations. *J Cereb Blood Flow Metab* 1985; 5:584–590.
14. Logan J, Fowler JS, Volkow ND, Wolf AP, Dewey SL, Schlyer DJ, MacGregor RR, Hitzemann R, Bendriem B, Gatley SJ. Graphical analysis of reversible radioligand binding from time-activity measurements applied to [*N*-^{11}C-methyl]-(-)-cocaine PET studies in human subjects. *J Cereb Blood Flow Metab* 1990; 10:740–747.
15. Logan J. Graphical analysis of PET data applied to reversible and irreversible tracers. *Nucl Med Biol* 2000; 27:661–670.
16. Miller GG, Ngan-Lee J, Chapman JD. Intracellular localization of radioactively labeled misonidazole in EMT-6-tumor cells in vitro. *Int J Radiat Oncol Biol Phys* 1982; 8:741–744.
17. Chapman JD, Zanzonico P, Ling CC. On measuring hypoxia in individual tumors with radiolabeled agents. *J Nucl Med* 2001; 42:1653–1655.
18. Chapman JD, McPhee MS, Walz N, Chetner MP, Stobbe CC, Soderlind K, Arnfield M, Meeker BE, Trimble L, Allen PS. Nuclear magnetic resonance spectroscopy and sensitizer-adduct measurements of photodynamic therapy-induced ischemia in solid tumors. *J Natl Cancer Inst* 1991; 83:1650–1659.
19. Iyer RV, Engelhardt EL, Stobbe CC, Schneider RF, Chapman JD. Preclinical assessment of hypoxic marker specificity and sensitivity. *Int J Radiat Oncol Biol Phys* 1998; 42:741–745.

20. Nordsmark M, Loncaster J, Chou SC, Havsteen H, Lindegaard JC, Davidson SE, Varia M, West C, Hunter R, Overgaard J, Raleigh JA. Invasive oxygen measurements and pimonidazole labeling in human cervix carcinoma. *Int J Radiat Oncol Biol Phys* 2001; 49:581–586.
21. Raleigh JA, Chou SC, Arteel GE, Horsman MR. Comparisons among pimonidazole binding, oxygen electrode measurements, and radiation response in C3H mouse tumors. *Radiat Res* 1999; 151:580–589.
22. Overgaard J, Horsman MR. Modification of hypoxia-induced radioresistance in tumors by the use of oxygen and sensitizers. *Semin Radiat Oncol* 1996; 6:10–21.
23. Overgaard J. Overcoming hypoxic cell radioresistance. In: Steel GG, ed. *Basic clinical radiobiology for radiation oncologists*. London: Edward Arnold; 1997:141–151.
24. Lewis JS, McCarthy DW, McCarthy TJ, Fujibayashi Y, Welch MJ. Evaluation of ^{64}Cu-ATSM in vitro and in vivo in a hypoxic tumor model. *J Nucl Med* 1999; 40:177–183.
25. Hartmann KA, van der Kleij AJ, Carl UM, Hulshof MC, Willers R, Sminia P. Effects of hyperbaric oxygen and normobaric carbogen on the radiation response of the rat rhabdomyosarcoma R1H(1). *Int J Radiat Oncol Biol Phys* 2001; 51:1037–1044.
26. Brown JM, Giaccia AJ. The unique physiology of solid tumors: opportunities (and problems) for cancer therapy. *Cancer Res* 1998; 58:1408–1416.